




## Article

# Hydrothermal Synthesis of MnO<sub>2</sub>/Reduced Graphene Oxide Composite for 4-Nitrophenol Sensing Applications

Praveen Kumar <sup>1,†</sup>, Mohd Quasim Khan <sup>2</sup>, Rais Ahmad Khan <sup>3</sup> , Khursheed Ahmad <sup>4,†</sup>   
and Haekyoung Kim <sup>4,\*</sup> 

<sup>1</sup> Department of Chemistry, Indian Institute of Technology Indore, Khandwa Road, Simrol, Indore 453552, Madhya Pradesh, India

<sup>2</sup> Department of Chemistry, M.M.D.C, Moradabad, M.J.P. Rohilkhand University, Bareilly 244001, Uttar Pradesh, India

<sup>3</sup> Department of Chemistry, College of Science, King Saud University, Riyadh 11451, Saudi Arabia

<sup>4</sup> School of Materials Science and Engineering, Yeungnam University, Gyeongsan 38541, Republic of Korea

\* Correspondence: hkkim@ynu.ac.kr

† These authors contributed equally to this work.

**Abstract:** Recently, the electrochemical sensing approach has attracted materials/electrochemical scientists to design and develop electrode materials for the construction of electrochemical sensors for the detection of para-nitrophenol (4-NP). In the present study, we have prepared a hybrid composite of MnO<sub>2</sub> and rGO (MnO<sub>2</sub>/rGO) using a hydrothermal approach. The morphological features of the prepared MnO<sub>2</sub>/rGO composite were studied by scanning electron microscopy, whereas the phase purity and formation of the MnO<sub>2</sub>/rGO composite were authenticated via the powder X-ray diffraction method. Energy-dispersive X-ray spectroscopy was also employed to analyze the elemental composition of the prepared MnO<sub>2</sub>/rGO composite. In further studies, a glassy carbon electrode (GCE) was modified with MnO<sub>2</sub>/rGO composite (MnO<sub>2</sub>/rGO/GCE) and explored as 4-nitrophenol (4-NP) sensor. The fabricated MnO<sub>2</sub>/rGO/GCE exhibited a reasonably good limit of detection of 0.09 μM with a sensitivity of 0.657 μA/μMcm<sup>2</sup>. The MnO<sub>2</sub>/rGO/GCE also demonstrates good selectivity, stability and repeatability in 50 cycles.

**Keywords:** MnO<sub>2</sub>/rGO composite; 4-NP; cyclic voltammetry; electrochemical sensor



**Citation:** Kumar, P.; Khan, M.Q.; Khan, R.A.; Ahmad, K.; Kim, H. Hydrothermal Synthesis of MnO<sub>2</sub>/Reduced Graphene Oxide Composite for 4-Nitrophenol Sensing Applications. *Inorganics* **2022**, *10*, 219. <https://doi.org/10.3390/inorganics10120219>

Academic Editor: Zuzana Vlckova Zivcova

Received: 10 October 2022

Accepted: 22 November 2022

Published: 24 November 2022

**Publisher's Note:** MDPI stays neutral with regard to jurisdictional claims in published maps and institutional affiliations.



**Copyright:** © 2022 by the authors. Licensee MDPI, Basel, Switzerland. This article is an open access article distributed under the terms and conditions of the Creative Commons Attribution (CC BY) license (<https://creativecommons.org/licenses/by/4.0/>).

## 1. Introduction

In the past few decades, environmental pollution has become one of the major threats globally. There are a large number of toxic and hazardous compounds which have negative influences on human health and the environment [1]. Nitrophenols are widely used in various industries manufacturing rubber, pesticides, petrochemical products, plastics, dyes, fungicides, and paints [2–8]. Nitrophenols are the major water pollutants that are directly released to the water reservoir bodies from various industries as discharged products. The presence of nitrophenols in water reservoir bodies and the environment can change the biological and chemical nature of the terrestrial environment and water [1,5]. It has been found that even the presence of nitrophenols with low concentrations could significantly influence the human being and environment [3]. The environment and human health may be at risk from the widespread use of 4-NP [3]. Excessive exposure to 4-NP may damage the kidney, liver, and human central nervous system, including some other health problems such as headaches, skin irritation, cyanosis, methemoglobinemia, sleepiness, and nausea [2,5,8]. The soil, crops, and water bodies can all be impacted by the presence of 4-NP [2]. These are serious issues; hence it is vital to regulate the use of 4-NP in all areas, including food, soil, and water. In this context, the sensitive detection of 4-NP is essential [4]. Numerous analytical techniques, including fluorescence, spectrofluorimetric, optical spectroscopy, enzyme-linked immunosorbent assay, liquid

chromatography, spectrophotometry, gas chromatography, capillary zone electrophoresis, and high-performance liquid chromatography, have been explored for the detection of 4-NP [9–17]. However, all of these approaches are time-consuming and have their own drawbacks/limitations [18,19]. Recently, the electrochemical technique has gained much attention because of its fast detection response, excellent selectivity, high sensitivity and cost-effectiveness [20–23]. Electrochemical sensing approach has been employed as a detection technique that records the signal during the oxidation/reduction process [24,25]. The electrochemical sensors need electro-catalysts that catalyze the oxidation/reduction of 4-NP. In previous years, various semiconducting metal oxides (manganese oxide ( $\text{MnO}_2$ ), zinc oxide ( $\text{ZnO}$ ), nickel oxide ( $\text{NiO}$ ), copper oxide ( $\text{CuO}$ ), magnesium oxide ( $\text{MgO}$ )) and perovskite materials, including  $\text{SrTiO}_3$  have been employed as electro-catalysts for the development of electrochemical sensor [26–31].  $\text{MnO}_2$  is one of the promising candidates and has been extensively used in supercapacitors, wastewater treatment, catalytic sensors, and solar cells due to its cost-effectiveness, high energy density, natural abundance, and non-toxicity [32]. It has been reported that pristine  $\text{MnO}_2$  has low conductivity, which can influence the electrochemical performance of  $\text{MnO}_2$ -based devices.

In this regard, recent reports showed that the incorporation of Pd with  $\text{MnO}_2$  improves the electrochemical performance of  $\text{MnO}_2$ -based devices [33]. Ahmad et al. also introduced copper to the  $\text{MnO}_2$  to enhance the electrochemical activity of the  $\text{MnO}_2$ -based sensors [26]. In some other works, it has been studied that the incorporation of carbon-based materials such as reduced graphene oxide (rGO) can significantly improve the conductive nature of the  $\text{MnO}_2$ . rGO has excellent mechanical stability, good conductivity, thermal stability, and high surface area [34,35]. rGO has been extensively used as conductive support to improve the conductive nature of poor semiconducting metal oxides [36,37]. It is clear that rGO is one of the most suitable candidates for improving the conductivity of  $\text{MnO}_2$  [35]. Jaiswal et al. [35] prepared  $\text{MnO}_2$ /rGO composite and used it as electrode material for the construction of nitrite sensors. The fabricated nitrite sensor exhibited good electrocatalytic properties for the detection of nitrite. This can be attributed to the synergistic effects between  $\text{MnO}_2$  and rGO. This clearly showed that  $\text{MnO}_2$  has good electro-catalytic properties, whereas rGO has a good surface area and conductivity [35]. This indicated that the combination of  $\text{MnO}_2$  and rGO may be useful for the development of electrochemical sensors.

Herein, we have fabricated a hybrid composite of  $\text{MnO}_2$  and rGO using the hydrothermal method. Further, a 4-NP electrochemical sensor was fabricated using the drop-cast method. The developed sensor exhibits a reasonable limit of detection, decent sensitivity, and good selectivity and stability.

## 2. Experimental Section

All the used materials and chemicals were bought from Loba, SRL, TCI, Alfa-Aesar, Sigma, and Merck and used without any further purification.

### 2.1. Synthesis of Graphene Oxide (GO)

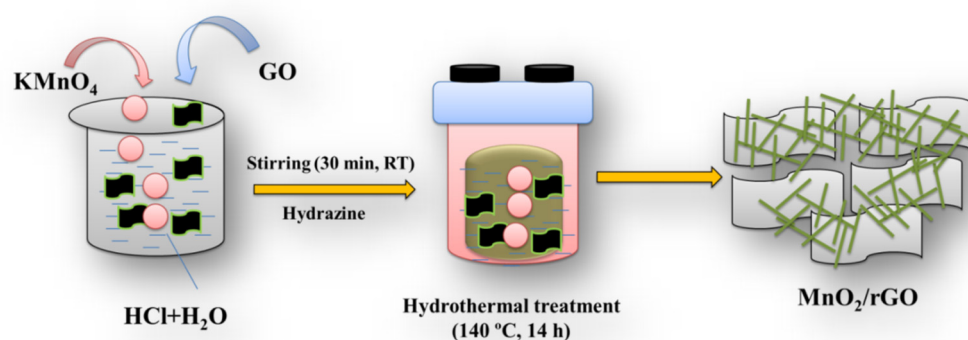
In accordance with the earlier study, GO was synthesized using the renowned Hummer's Method [38]. In brief, 23.0 mL  $\text{H}_2\text{SO}_4$  was added to 1.0 g of graphite flakes and 0.5 g of  $\text{NaNO}_3$ , which were thoroughly mixed before being kept at room temperature for 30 min. The exothermic reaction was controlled by using ICE (temperature below 20 °C), adding  $\text{KMnO}_4$  (3.0 g) gradually, which was then continuously stirred for an entire night at room temperature. After adding, 60 mL of distilled water and 1.5 g of  $\text{KMnO}_4$  were gently added to the reaction mixture, which was then stirred once more for 14 h at room temperature. After completion, the mixture was allowed to cool, and 500 mL of DI water was added, along with 7 mL of 30%  $\text{H}_2\text{O}_2$ . After brief washing with 1M HCl, the resulting crude was repeatedly rinsed with water. To achieve the final product, the final crude was washed with extra D.I. water and dried at 50 °C for 6 h.

## 2.2. Synthesis of MnO<sub>2</sub>/rGO

The MnO<sub>2</sub>/rGO composite and MnO<sub>2</sub> were synthesized using a hydrothermal method. First, 3.5 mmol of KMnO<sub>4</sub> was added to the 25 mL of distilled water, and a few drops of HCl were added. This reaction mixture was stirred for a few minutes at room temperature. On the other side, GO (50 mg) was dispersed in 10 mL of distilled water (having hydrazine) using a sonication bath. The GO dispersion was added to the KMnO<sub>4</sub> solution and stirred for 0.5 h at RT. Further, this solution was added to the Teflon lining hydrothermal autoclave (100 mL capacity) and heated to 140° for 12–14 h. Once the reaction finished, it was allowed to cool down to room temperature before the crude product was separated using a centrifuge. The crude was thoroughly cleaned using DI water and ethanol and dried overnight (70 °C). MnO<sub>2</sub> was prepared under similar conditions without adding GO solution [32]. rGO was prepared according to a previous report [38].

## 2.3. Fabrication of Electrochemical Sensor

For the electrochemical investigations, three electrodes—counter electrode (platinum; Pt), reference electrode (Ag/AgCl), and working electrode (GCE) were utilized. A glassy carbon electrode (GCE) served as the working electrode for the sensing application. The surface of GCE was modified with prepared materials (Scheme 1). The MnO<sub>2</sub>, rGO, and MnO<sub>2</sub>/rGO coated electrodes are labeled as MnO<sub>2</sub>/GCE, rGO/GCE, and MnO<sub>2</sub>/rGO/GCE, respectively, which were employed as the working electrode. On the other hand, bare GCE was labeled as GCE. 0.1 M PBS of pH 7.0 was used for all the electrochemical studies. A computer-controlled Potentiostat was used for all of the electrochemical experiments (CH Instrument). The working electrodes (GCE) have a 3 mm-diameter geometrical area.



**Scheme 1.** Schematic diagram for the synthesis of MnO<sub>2</sub>/rGO composite.

## 3. Results and Discussion

### 3.1. General Characterization

In order to confirm the formation of the MnO<sub>2</sub>/rGO composite, we have obtained the X-ray diffraction (XRD) of the prepared powder sample of the MnO<sub>2</sub>/rGO composite (Rigaku, Japan, Instrument). The XRD of the MnO<sub>2</sub>/rGO composite was collected at the 2 $\theta$  of 10–80°. The collected XRD pattern of the MnO<sub>2</sub>/rGO composite has been displayed in Figure 1. Figure 1 demonstrates the presence of various diffraction peaks, which can be assigned to the (110), (200), (310), (211), (301), (411), (600), (521), (002), and (521) diffraction planes of MnO<sub>2</sub> (JCPDS number 44-0141). However, no diffraction peak related to the rGO could be observed. The XRD pattern of the pristine MnO<sub>2</sub> was also collected and has been incorporated in Figure 1. The XRD of MnO<sub>2</sub> exhibited the presence of various diffraction planes of (110), (200), (310), (211), (301), (411), (600), (521), (002), and (521). The XRD studies showed that the incorporation of rGO into MnO<sub>2</sub> changes the crystallinity of the prepared MnO<sub>2</sub>/rGO composite, which may be due to the amorphous nature of rGO. The XRD pattern rGO was also collected to verify the formation of rGO. The XRD data of the rGO has been presented in Figure S1 in the supporting information.

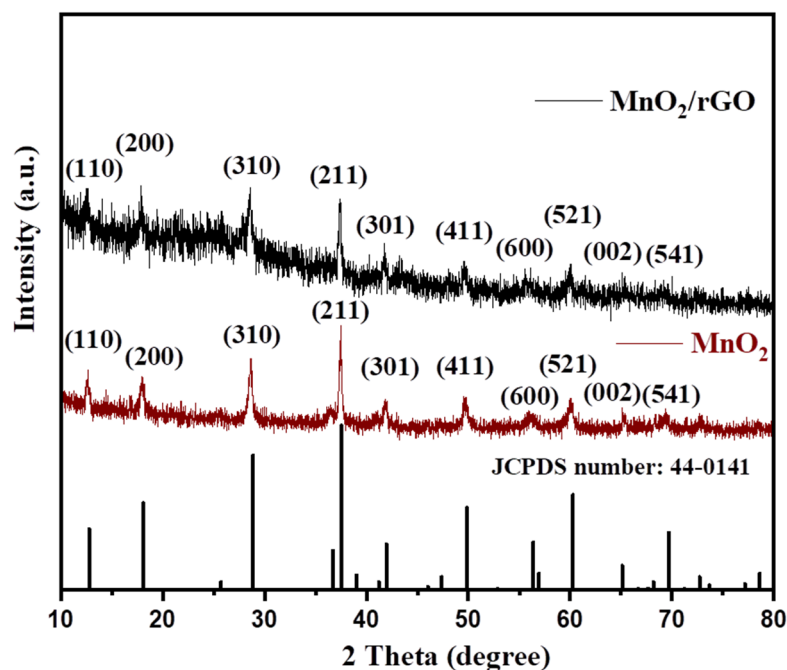


**Figure 1.** XRD pattern of MnO<sub>2</sub> and MnO<sub>2</sub>/rGO.

A clearly defined diffraction plane (002) was visible in the rGO XRD pattern. This confirmed the preparation of MnO<sub>2</sub>, rGO, and MnO<sub>2</sub>/rGO composite. The Raman spectra (Horiba-Scientific Instrument; laser wavelength = 532 nm; grating = 1800 gr/mm) of the rGO, MnO<sub>2</sub> and MnO<sub>2</sub>/rGO were also obtained. The obtained results showed that MnO<sub>2</sub> has two peaks at 569.4 and 640.1 cm<sup>-1</sup>, which can be assigned to the symmetric stretching vibration of the MnO<sub>6</sub> octahedral group and the stretching vibration of the Mn-O bond, respectively (Figure S2). Raman spectrum of rGO exhibits the presence of D and G bands. The Raman spectrum of MnO<sub>2</sub>/rGO showed Raman peaks for MnO<sub>2</sub> along with D and G bands of rGO (Figure S2). This suggested the formation of MnO<sub>2</sub>/rGO composite.

The morphology of electrode materials can significantly alter the performance of the electrochemical devices.

Thus, morphological characteristics of the prepared MnO<sub>2</sub> and MnO<sub>2</sub>/rGO composite were also studied. The morphological features of the MnO<sub>2</sub> and MnO<sub>2</sub>/rGO composite were investigated by recording scanning electron microscopic (SEM) images on Hitachi (S-4800) SEM instrument. The SEM pictures of the MnO<sub>2</sub> and MnO<sub>2</sub>/rGO composite are presented in Figure 2. Figure 2a demonstrates the presence of rod-like surface properties of the prepared MnO<sub>2</sub>. Similarly, Figure 2b shows that MnO<sub>2</sub> rods are present on rGO sheets. Thus, it can be understood that rGO has a sheet-like morphology on which rod-like MnO<sub>2</sub> has been grown via the hydrothermal method (Figure 2b). Transmission electron microscopy (TEM) was also used to further characterize the prepared MnO<sub>2</sub>/rGO composite. The obtained TEM image of the MnO<sub>2</sub>/rGO composite has been presented in Figure S3, which indicates that MnO<sub>2</sub> rods are present on the rGO surface. The determination of the elemental composition of the MnO<sub>2</sub> and MnO<sub>2</sub>/rGO composites is necessary to verify the formation of the MnO<sub>2</sub> and MnO<sub>2</sub>/rGO composites. Hence, energy-dispersive X-ray spectroscopy (EDX; Horiba instrument) was explored to authenticate the formation of MnO<sub>2</sub> and MnO<sub>2</sub>/rGO composite. The obtained EDX results of the MnO<sub>2</sub> and MnO<sub>2</sub>/rGO composite are presented in Figure 3a–d. The EDX spectrum of MnO<sub>2</sub> indicated the presence of Mn and O elements (Figure 3b), which suggested the formation of MnO<sub>2</sub>. On the other side, the EDX spectrum of MnO<sub>2</sub>/rGO indicated the presence of Mn, O, and C elements and authenticated the formation of the MnO<sub>2</sub>/rGO composite (Figure 3d). In the MnO<sub>2</sub>/rGO composite, C, Mn, and O elements have weight percentages of 9.78%, 61.13%, and 29.09%, respectively.

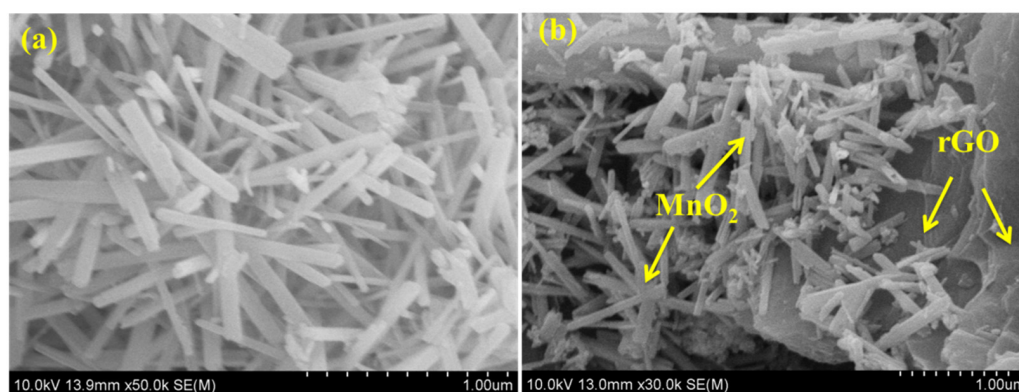


Figure 2. SEM images of MnO<sub>2</sub> (a) and MnO<sub>2</sub>/rGO (b).

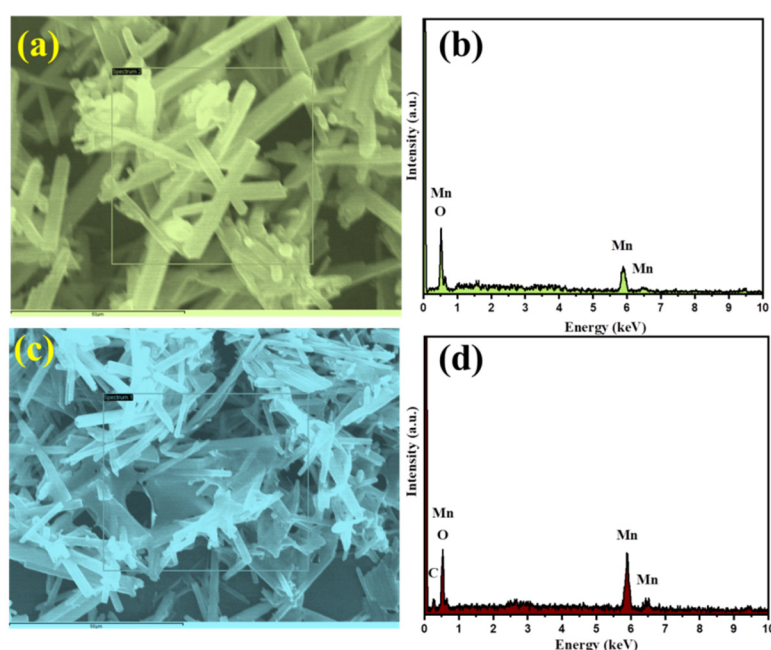


Figure 3. EDX analysis of MnO<sub>2</sub> (a,b) and MnO<sub>2</sub>/rGO (c,d).

Thus, it can be said that MnO<sub>2</sub> and MnO<sub>2</sub>/rGO composite are prepared successfully via the hydrothermal approach with good phase purity.

### 3.2. Electrochemical Performance

To calculate the electrochemically active surface area (ECSA) of the GCE, MnO<sub>2</sub>/GCE, rGO/GCE, and MnO<sub>2</sub>/rGO/GCE, CVs curves were recorded in 5 mM [Fe(CN)<sub>6</sub>]<sup>3−/4−</sup> redox couple scan rate of 100 mVs<sup>−1</sup> (Figure S4). The electrochemically active surface area of the GCE, MnO<sub>2</sub>/GCE, rGO/GCE and MnO<sub>2</sub>/rGO/GCE were calculated by using the Randles–Sevcik equation given below,

$$I_p = 2.69 \times 10^5 AD^{1/2} n^{3/2} \nu^{1/2} C \quad (1)$$

In Equation (1),  $I_p$  is the peak current,  $A$  is the ECSA (to be calculated),  $\nu$  is scan rate (V/s), and  $n$  = no. of electrons ( $n = 1$ ) for redox couple [Fe(CN)<sub>6</sub>]<sup>3−/4−</sup>,  $C$  is the concentration (mol/L), and  $D$  is the diffusion coefficient ( $6.7 \times 10^{-6}$  cm<sup>2</sup> s<sup>−1</sup>). The ECSAs of the bare GCE, MnO<sub>2</sub>/GCE, rGO/GCE, and MnO<sub>2</sub>/rGO/GCE were 0.07, 0.078, 0.084, and 0.097 cm<sup>2</sup>, respectively.

By recording the CVs of the GCE, MnO<sub>2</sub>/GCE, rGO/GCE, and MnO<sub>2</sub>/rGO/GCE in 50 µM 4-NP (scan rate = 50 mV/s), the electrochemical sensing activity of the GCE,

MnO<sub>2</sub>/GCE, rGO/GCE, and MnO<sub>2</sub>/rGO/GCE was assessed. Figure 4a shows the calculated CV curves for the GCE, MnO<sub>2</sub>/GCE, rGO/GCE, and MnO<sub>2</sub>/rGO/GCE in 50 μM 4-NP. The CV findings indicated low electro-catalytic current response for GCE whereas MnO<sub>2</sub>/rGO produced a somewhat better electro-catalytic current. However, rGO/GCE exhibits a better current response compared to the GCE or MnO<sub>2</sub>/GCE. But the highest electro-catalytic current was observed for MnO<sub>2</sub>/rGO/GCE, which may be due to the presence of synergistic effects between MnO<sub>2</sub> and rGO. It can be clearly seen that MnO<sub>2</sub>/rGO/GCE possesses the highest sensing property for the sensing of 50 μM 4-NP compared to the GCE, MnO<sub>2</sub>/GCE or rGO/GCE (Figure 4a).

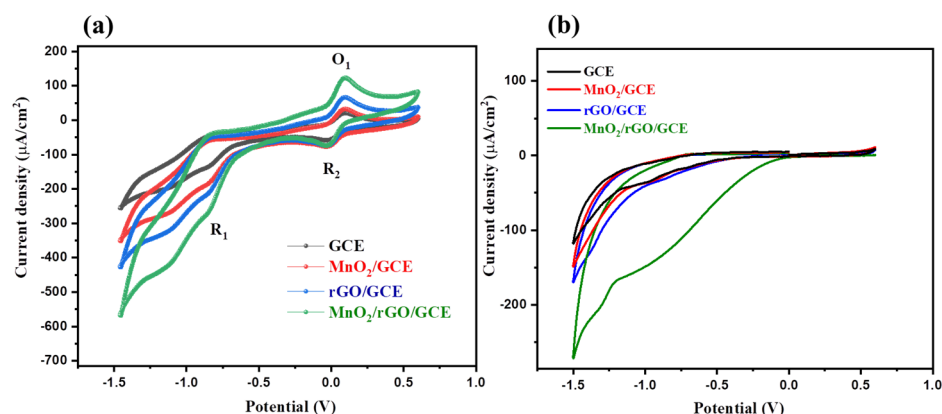
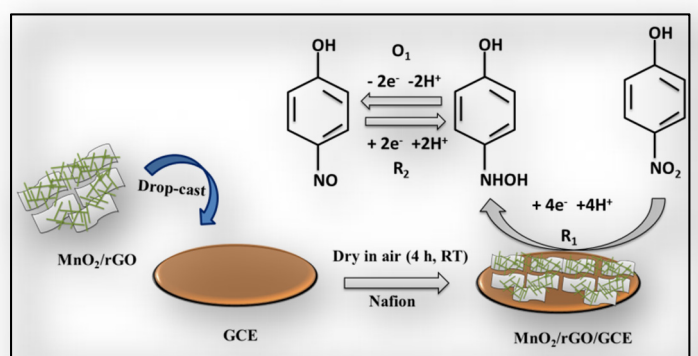


**Figure 4.** CV of GCE, MnO<sub>2</sub>/GCE, rGO/GCE and MnO<sub>2</sub>/rGO/GCE in the presence (a) and absence (b) of 50 μM 4-NP (scan rate = 50 mV/s).

In the absence of 4-NP, the CV responses of the GCE, MnO<sub>2</sub>/GCE, rGO/GCE, and MnO<sub>2</sub>/rGO/GCE were taken at a scan rate of 50 mV/s in 0.1 M PBS at pH 7.0. (Figure 4b). The obtained findings demonstrated that, in comparison to the other electrodes, MnO<sub>2</sub>/rGO/GCE had the highest electro-catalytic activity. As a result, we used MnO<sub>2</sub>/rGO/GCE as a possible working electrode for more CV research. The CV results showed the presence of one oxidation peak (O<sub>1</sub>) and two reduction peaks (R<sub>1</sub> and R<sub>2</sub>) for the detection of 4-NP, which may be related to the oxidation and reduction of the 4-NP (Scheme 2) during the electrochemical process/reactions. The applied scan rate can significantly alter the current response of the MnO<sub>2</sub>/rGO/GCE. Thus, it is necessary to check the influence of different applied scan rates on the electro-catalytic behavior of the MnO<sub>2</sub>/rGO/GCE. In this regard, CV graphs of the MnO<sub>2</sub>/rGO/GCE were recorded at various scan rates of 50–500 mV/s in a fixed concentration of 4-NP (50 μM).



**Scheme 2.** The schematic diagram shows the construction and working of the 4-NP sensor.

The obtained CV results of the MnO<sub>2</sub>/rGO/GCE at various scan rates (50–500 mV/s) are presented in Figure 5a. With regard to the scan rate, it can be seen that the MnO<sub>2</sub>/rGO/GCE's

current response grows (Figure 5a) with increasing concentration. According to the calibration plot between the current response and the scan rate's square root, the current response appears to grow linearly (Figure 5b).

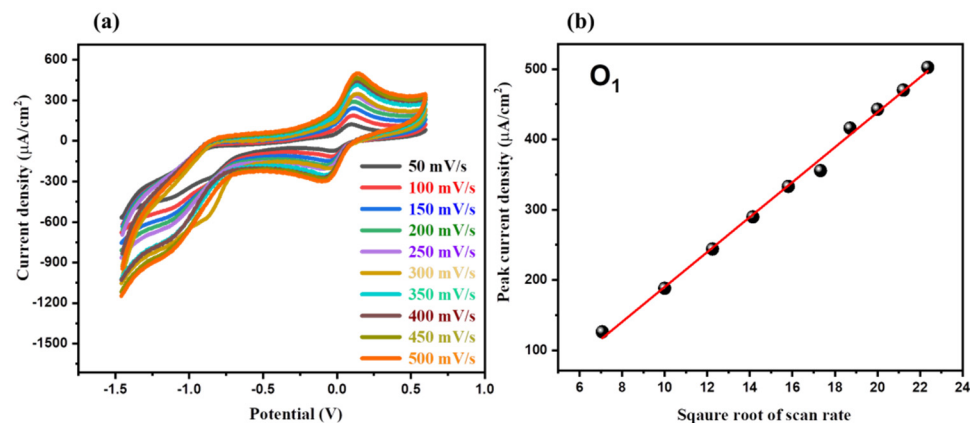


**Figure 5.** CV (a) of MnO<sub>2</sub>/rGO/GCE in 50 μM 4-NP (PBS = 0.1 M; pH = 7.0) at various scan rates (50–500 mV/s). Calibration plot (b) between the peak current and square root of various scan rates.

Recently, the LSV method has received enormous attention for electrochemical sensing applications. In our study, we also adopted the LSV technique for the detection of 4-NP. In the presence of 50 μM 4-NP and a scan rate of 50 mV/s, the LSV graphs of the GCE, MnO<sub>2</sub>/GCE, rGO/GCE, and MnO<sub>2</sub>/rGO/GCE were obtained. Figure 6 shows the obtained LSV curves of the GCE, MnO<sub>2</sub>/GCE, rGO/GCE, and MnO<sub>2</sub>/rGO/GCE. The GCE has the lowest current response, while MnO<sub>2</sub>/GCE showed an improved current response for the detection of 50 μM 4-NP (Figure 6). Further enhancement in the current response of the rGO/GCE was also observed, which may be due to the conductive nature of rGO. The MnO<sub>2</sub>/rGO/GCE exhibited the highest current response compared to the GCE, MnO<sub>2</sub>/GCE or rGO/GCE (Figure 6). The presence of a synergistic interaction between MnO<sub>2</sub> and rGO may be responsible for this increased current response (Figure 6). Further LSV research was conducted using the MnO<sub>2</sub>/rGO/GCE. We have also prepared MnO<sub>2</sub>/rGO composite using different amounts of GO (5 mg, 15 mg, and 35 mg). Further, GCE was modified with prepared different MnO<sub>2</sub>/rGO composites, and their electro-catalytic properties were examined using LSV. The obtained results are presented in Figure S5. The observations showed that MnO<sub>2</sub>/rGO composite prepared with 35 mg GO has good electrocatalytic activity but is still lower than that of the MnO<sub>2</sub>/rGO composite prepared with 50 mg GO. Furthermore, we have also physically mixed 50 mg of GO with 100 mg MnO<sub>2</sub> using mortar and pestle. The GCE was also modified with physically mixed MnO<sub>2</sub>/rGO, and its electrocatalytic properties were also checked under similar conditions via the LSV method. The obtained LSV result is presented in Figure S6. The observations showed that physically mixed MnO<sub>2</sub>/rGO has decent performance but is still lower than that of the hydrothermally prepared MnO<sub>2</sub>/rGO composite.

The concentration of 4-NP can influence the current response of the MnO<sub>2</sub>/rGO/GCE. In this regard, we have obtained LSV graphs of the MnO<sub>2</sub>/rGO/GCE at various concentrations of 4-NP (0, 0.3 μM, 2.5 μM, 6.5 μM, 11.5 μM, 17.5 μM, 25.5 μM, 32.5 μM, 41.5 μM, and 50 μM (scan rate = 50 mV/s).

The obtained LSV results of the MnO<sub>2</sub>/rGO/GCE at various concentrations of 4-NP are depicted in Figure 7a. The observations indicated that the electro-current of the MnO<sub>2</sub>/rGO/GCE increases with respect to the concentration of the 4-NP. Figure 7b is a calibration curve showing the relationship between the peak current density response and 4-NP concentration. The LSV findings indicated that the current response rises linearly with rising 4-NP concentration.

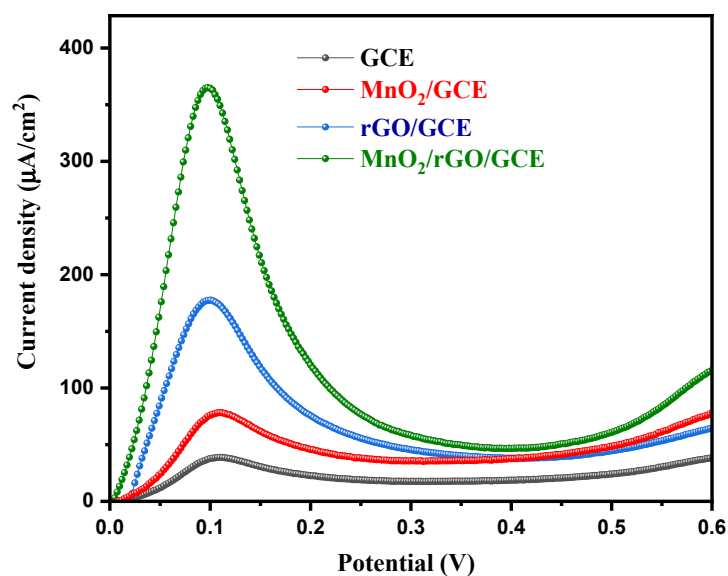


**Figure 6.** LSV of GCE,  $\text{MnO}_2/\text{GCE}$ ,  $\text{rGO}/\text{GCE}$  and  $\text{MnO}_2/\text{rGO}/\text{GCE}$  in  $50 \mu\text{M}$  4-NP (PBS =  $0.1 \text{ M}$ ; pH =  $7.0$ ; scan rate =  $50 \text{ mV/s}$ ).

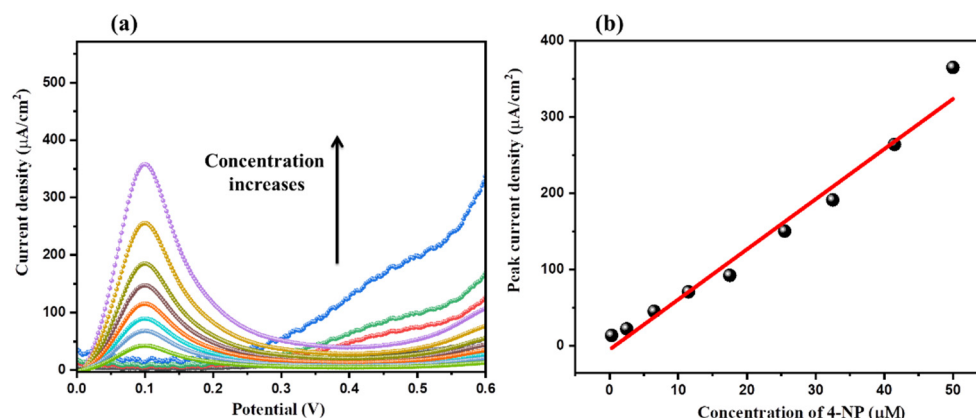


**Figure 7.** LSV (a) of  $\text{MnO}_2/\text{rGO}/\text{GCE}$  in various concentrations ( $0, 0.3 \mu\text{M}, 2.5 \mu\text{M}, 6.5 \mu\text{M}, 11.5 \mu\text{M}, 17.5 \mu\text{M}, 25.5 \mu\text{M}, 32.5 \mu\text{M}, 41.5 \mu\text{M}$  and  $50 \mu\text{M}$ ) of 4-NP (scan rate =  $50 \text{ mV/s}$ ). The calibration curve (b) of the peak current density versus the concentration of 4-NP.

The selectivity of the sensor is an important consideration when evaluating how well an active material can detect toxic materials. In this context, the  $\text{MnO}_2/\text{rGO}/\text{GCE}$  selectivity test toward the sensing of 4-NP in the presence of several interfering species was conducted using the LSV approach. Figure 8 shows the LSV graphs of the  $\text{MnO}_2/\text{rGO}/\text{GCE}$  recorded at a scan rate of  $50 \text{ mV/s}$  in the presence of  $50 \mu\text{M}$  4-NP and  $50 \mu\text{M}$  4-NP +  $200 \mu\text{M}$  interfering species (urea, uric acid, glucose, dopamine, catechol, ascorbic acid, hydroquinone, hydrazine, and  $\text{H}_2\text{O}_2$ ).

The LSV results showed that the presence of interfering species could not alter the current response or potential, which suggested the good selective nature of  $\text{MnO}_2/\text{rGO}/\text{GCE}$  for the sensing of 4-NP in the presence of various interfering species (Figure 8). The repeatability and stability of the  $\text{MnO}_2/\text{rGO}/\text{GCE}$  were also evaluated using the LSV method. Fifty consecutive LSV graphs of the  $\text{MnO}_2/\text{rGO}/\text{GCE}$  were recorded in the presence of  $50 \mu\text{M}$  4-NP at a scan rate of  $50 \text{ mV/s}$ . The obtained LSV graphs are presented in Figure 9.



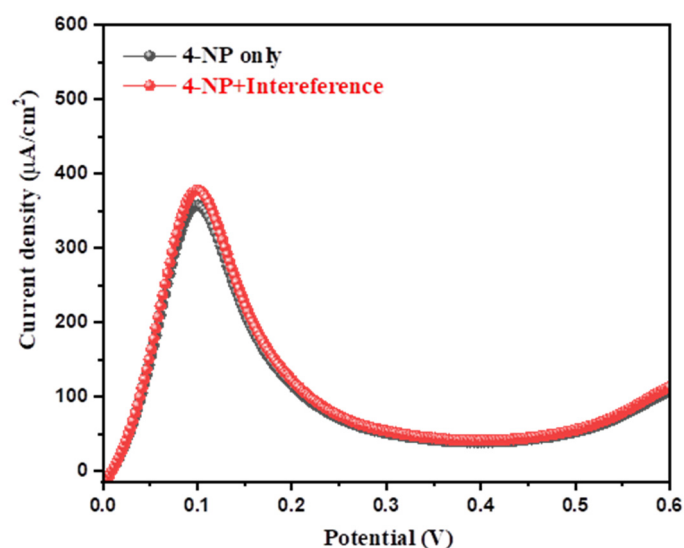


**Figure 8.** LSV of  $\text{MnO}_2/\text{rGO}/\text{GCE}$  in  $50 \mu\text{M}$  4-NP and  $50 \mu\text{M}$  4-NP +  $200 \mu\text{M}$  interference species (urea, uric acid, glucose, dopamine, catechol, ascorbic acid, hydroquinone, hydrazine, and  $\text{H}_2\text{O}_2$ ) (scan rate =  $50 \text{ mV/s}$ ).

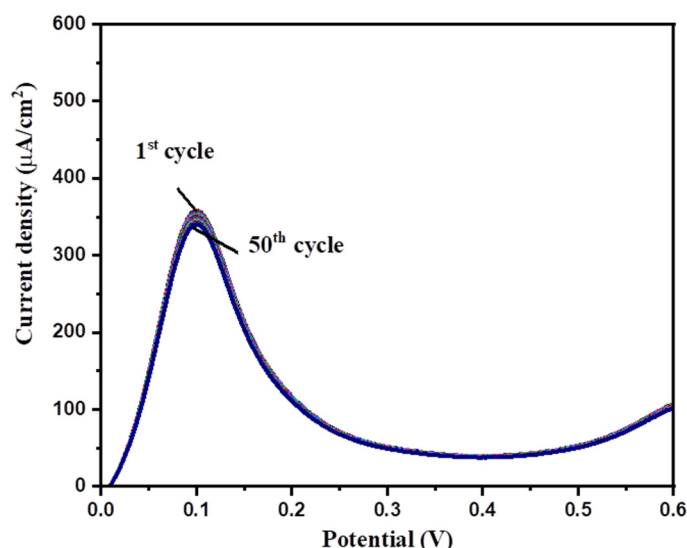


**Figure 9.** Fifty consecutive LSV curves of  $\text{MnO}_2/\text{rGO}/\text{GCE}$  in  $50 \mu\text{M}$  4-NP (scan rate =  $50 \text{ mV/s}$ ).

The acquired findings demonstrated that little fluctuations in current responsiveness were seen, indicating strong cyclic stability and repeatability up to 50 cycles. Under comparable circumstances, the repeatability of the  $\text{MnO}_2/\text{rGO}/\text{GCE}$  was also investigated. Four freshly prepared  $\text{MnO}_2/\text{rGO}/\text{GCE}$ s were used to investigate the reproducibility studies. The observations showed decent results, which suggested good reproducibility.

The probable sensing mechanism for the detection of 4-NP using  $\text{MnO}_2/\text{rGO}/\text{GCE}$  can be explained according to the reported literature [31]. In Scheme 2, the likely detection process for 4-NP is depicted. The oxidation and reduction reactions of the 4-NP are indicated in Scheme 2 by  $\text{O}_1$  and  $\text{R}_1$ ,  $\text{R}_2$ . Firstly, reduction ( $\text{R}_1$ ) is responsible for the transformation of 4-NP into p-hydroxyl-amino-phenol ( $\text{R}_1$ ).

In a subsequent redox reaction, the p-hydroxyl-amino-phenol is oxidized ( $\text{O}_1$ ) and transformed into the p-nitroso-phenol, and reversible reduction ( $\text{R}_2$ ) completes the redox reaction (Scheme 2). The performance of  $\text{MnO}_2/\text{rGO}/\text{GCE}$  was then evaluated in terms of stability, repeatability, and selectivity for sensing 4-NP. Additional calculations of crucial

parameters, such as the sensitivity and the detection limit (LOD), were made in order to assess the performance, accuracy, and application of the results.

As shown below, the detection limit (LoD) and Sensitivity were determined using the modified electrode's Equations (2) and (3).

$$\text{LoD} = 3.3 (\sigma/S) \quad (2)$$

$$\text{Sensitivity} = \text{slope/area} \quad (3)$$

( $\sigma$  is the standard deviation or error; S is the slope, and the area of the electrode is  $0.07 \text{ cm}^2$ ).

The calculated LoD and sensitivity of the  $\text{MnO}_2/\text{rGO}/\text{GCE}$  are summarized in Table 1.

In the past years, various 4-NP sensors have been reported. In this connection, Gao et al. [39] prepared  $\text{MnO}_2$  nanotubes and investigated the role of  $\text{MnO}_2$  nanotubes as an electrochemical sensor for the detection of 4-NP. The developed sensor showed an LoD of 0.1 mM. In another report, Zhang et al. [40] also developed a 4-NP sensor using  $\text{Mg}(\text{Ni})\text{FeO}$  as electrode material which demonstrated LoD of  $0.2 \mu\text{M}$ . A flower-shaped zinc oxide-based nanomaterial was also synthesized by Yu et al. [41] and fabricated a 4-NP sensor. This 4-NP sensor displayed an LoD of  $13 \mu\text{M}$ . Chu et al. [42] also coated nano-gold particles on GCE for electrochemical sensing of 4-NP and reported an LoD of  $8 \mu\text{M}$ . Yang et al. [43] also reported a good LoD of  $0.4 \mu\text{M}$  for multi-walled carbon nanotube-modified GCEs. A subsequent study of silver particle-modified GCE showed an LoD of  $0.5 \mu\text{M}$  [44]. In other reports, palladium-graphene composite/poly(N-isopropylacrylamide) based sensor exhibited good LoD of  $0.1 \mu\text{M}$  [45] whereas  $\text{SnO}_2@ZIF-8/\text{gC}_3\text{N}_4$  nanohybrids based sensor showed LoD of  $0.565 \mu\text{M}$  [46]. In another recent report, MWCNTs/ $\text{MnO}_2$ -based sensors also showed LoDs of  $0.64 \mu\text{M}$  [47]. The interesting LoD of  $0.16 \mu\text{M}$  was also reported for the sensing of 4-NP using  $\text{Ti}_3\text{C}_2\text{T}_x/\text{GR}/\text{GCE}$  [48]. P-doped  $\text{Fe}/\text{Fe}_3\text{O}_4@\text{C}$  based 4-NP sensor showed LoD of  $0.462 \mu\text{M}$  [49] while  $\text{Ti}_3\text{C}_2\text{T}_x$  MXene-based sensor showed LoD of  $0.11 \mu\text{M}$  [50]. Dighole et al. [51] also explored the potential role of bismuth oxide/MWCNTs as 4-NP sensing material and obtained a good LoD of  $0.1 \mu\text{M}$ . Our obtained LoD is comparable with previous reports, as listed in Table 1. In the present work, the better electro-catalytic properties of  $\text{MnO}_2$  and the high surface area of rGO with good conductivity improved the detection of 4-NP.

**Table 1.** Comparison of reported 4-NP sensors with  $\text{MnO}_2/\text{rGO}/\text{GCE}$ 's performance [39–44].

Material	LoD ( $\mu\text{M}$ )	Sensitivity ( $\mu\text{A}/\mu\text{Mcm}^2$ )	References
$\alpha\text{-MnO}_2$ nanotube/GCE	100	0.19	[39]
$\text{Mg}(\text{Ni})\text{FeO}/\text{CPE}$	0.2	0.81	[40]
$\text{ZnO}/\text{GCE}$	13	0.404	[41]
Nanogold/GCE	8	-	[42]
MWCNT/GCE	0.4	-	[43]
Silver particles/GCE	0.5	-	[44]
palladium-graphene composite/poly(N-isopropylacrylamide)	0.1	-	[45]
$\text{SnO}_2@ZIF-8/\text{gC}_3\text{N}_4$ nanohybrids	0.565	2.63	[46]
MWCNTs/ $\text{MnO}_2$	0.64	0.186	[47]
$\text{Ti}_3\text{C}_2\text{T}_x/\text{GR}/\text{GCE}$	0.16	-	[48]
P-doped $\text{Fe}/\text{Fe}_3\text{O}_4@\text{C}$	0.462	-	[49]
$\text{Ti}_3\text{C}_2\text{T}_x$ MXene	0.11	1.22	[50]
$\text{Bi}_2\text{O}_3@\text{MWCNTs}$	0.1	-	[51]
<b><math>\text{MnO}_2/\text{rGO}/\text{GCE}</math></b>	<b>0.09</b>	<b>0.657</b>	<b>Praveen et al.</b>

#### 4. Conclusions

It can be summarized that MnO<sub>2</sub>/rGO composite has been obtained using a hydrothermal approach. Further, the physiochemical properties of the prepared MnO<sub>2</sub>/rGO composite were checked by various advanced techniques, including scanning electron microscopy and X-ray diffraction techniques. The *para*-nitrophenol (4-NP) sensor was constructed by modifying the surface of the glassy carbon electrode with the prepared MnO<sub>2</sub>/rGO composite as an electrode modifier. Due to the beneficial interactions (synergistic) between MnO<sub>2</sub> and rGO, the fabricated 4-NP sensor had an excellent detection limit. The 4-NP sensor that was built demonstrated high stability and selectivity when it came to sensing 4-NP.

**Supplementary Materials:** The following supporting information can be downloaded at: <https://www.mdpi.com/article/10.3390/inorganics10120219/s1>, Figure S1: XRD of rGO; Figure S2: Raman of MnO<sub>2</sub>, rGO and MnO<sub>2</sub>/rGO; Figure S3: TEM of MnO<sub>2</sub>/rGO; Figure S4: CV responses; Figure S5: LSV responses; Figure S6: LSV responses.

**Author Contributions:** Conceptualization, P.K. and K.A.; methodology, K.A. and M.Q.K.; formal analysis, P.K., K.A. and M.Q.K.; investigation, P.K. and K.A.; resources, R.A.K. and H.K.; writing—original draft preparation, P.K., M.Q.K. and K.A.; writing—review and editing, R.A.K. and H.K.; supervision, R.A.K. and H.K.; funding acquisition, R.A.K. and H.K. All authors have read and agreed to the published version of the manuscript.

**Funding:** This research received no external funding.

**Data Availability Statement:** Not applicable.

**Acknowledgments:** R.A.K. acknowledged researchers supporting project number (RSP-2021/400), King Saud University, Riyadh, Saudi Arabia. P.K. thanks DST-Inspire, for the PhD fellowship. This work was supported by the Korea Innovation Foundation (INNOPOLIS) grant funded by the Korean government (MSIT; 2020-DD-UP-0278) and the National Research Foundation of Korea (NRF) grant funded by the Korean government (MSIT; No. 2019R1A5A8080290).

**Conflicts of Interest:** The authors declare no conflict of interest.

#### References

1. Singh, K.; Ibrahim, A.A.; Umar, A.; Kumar, A.; Chaudhary, G.R.; Singh, S.; Mehta, S.K. Synthesis of CeO<sub>2</sub>-ZnO Nanoellipsoids as Potential Scaffold for the Efficient Detection of 4-Nitrophenol. *Sens. Actuators B Chem.* **2014**, *202*, 1044–1050. [[CrossRef](#)]
2. Ahmad, N.; Al-Fatesh, A.S.; Wahab, R.; Alam, M.; Fakeeha, A.H. Synthesis of Silver Nanoparticles Decorated on Reduced Graphene Oxide Nanosheets and Their Electrochemical Sensing towards Hazardous 4-Nitrophenol. *J. Mater. Sci. Mater. Electron.* **2020**, *31*, 11927–11937. [[CrossRef](#)]
3. Al-Kahtani, A.A.; Almuqati, T.; Alhokbany, N.; Ahamad, T.; Naushad, M.; Alshehri, S.M. A Clean Approach for the Reduction of Hazardous 4-Nitrophenol Using Gold Nanoparticles Decorated Multiwalled Carbon Nanotubes. *J. Clean. Prod.* **2018**, *191*, 429–435. [[CrossRef](#)]
4. Dai, H.; Deng, Z.; Zeng, Y.; Zhang, J.; Yang, Y.; Ma, Q.; Hu, W.; Guo, L.; Li, L.; Wan, S.; et al. Highly Sensitive Determination of 4-Nitrophenol with Coumarin-Based Fluorescent Molecularly Imprinted Poly (Ionic Liquid). *J. Hazard. Mater.* **2020**, *398*, 122854. [[CrossRef](#)]
5. Ding, Q.; Kang, Z.; Cao, L.; Lin, M.; Lin, H.; Yang, D.-P. Conversion of Waste Eggshell into Difunctional Au/CaCO<sub>3</sub> Nanocomposite for 4-Nitrophenol Electrochemical Detection and Catalytic Reduction. *Appl. Surf. Sci.* **2020**, *510*, 145526. [[CrossRef](#)]
6. Jeyapragasam, T. Molybdenum Disulfide-Based Modifier for Electrochemical Detection of 4-Nitrophenol. *Ionics* **2018**, *24*, 4033–4041. [[CrossRef](#)]
7. Lu, W.; Ning, R.; Qin, X.; Zhang, Y.; Chang, G.; Liu, S.; Luo, Y.; Sun, X. Synthesis of Au Nanoparticles Decorated Graphene Oxide Nanosheets: Noncovalent Functionalization by TWEEN 20 in Situ Reduction of Aqueous Chloroaurate Ions for Hydrazine Detection and Catalytic Reduction of 4-Nitrophenol. *J. Hazard. Mater.* **2011**, *197*, 320–326. [[CrossRef](#)] [[PubMed](#)]
8. Manjula, N.; Chen, S.-M. Simple Strategy Synthesis of Manganese Cobalt Oxide Anchored on Graphene Oxide Composite as an Efficient Electrocatalyst for Hazardous 4-Nitrophenol Detection in Toxic Tannery Waste. *Microchem. J.* **2021**, *168*, 106514. [[CrossRef](#)]
9. Padilla-Sánchez, J.A.; Plaza-Bolaños, P.; Romero-González, R.; Garrido-Frenich, A.; Martínez Vidal, J.L. Application of a Quick, Easy, Cheap, Effective, Rugged and Safe-Based Method for the Simultaneous Extraction of Chlorophenols, Alkylphenols, Nitrophenols and Cresols in Agricultural Soils, Analyzed by Using Gas Chromatography–Triple Quadrupole-Mass Spectrometry/Mass Spectrometry. *J. Chromatogr. A* **2010**, *1217*, 5724–5731.

10. El-Shahawi, M.S.; Othman, A.M.; El-Houseini, M.E.; Nashed, B.; Elsofy, M.S. Spectrofluorimetric Method for Measuring the Activity of the Enzyme  $\alpha$ -L-Fucosidase Using the Ion Associate of 2-Chloro-4-Nitro Phenol–Rhodamine-B. *Talanta* **2009**, *80*, 19–23. [[CrossRef](#)]
11. Salcedo, G.M.; Kupski, L.; Degang, L.; Marube, L.C.; Caldas, S.S.; Primel, E.G. Determination of Fifteen Phenols in Wastewater from Petroleum Refinery Samples Using a Dispersive Liquid–Liquid Microextraction and Liquid Chromatography with a Photodiode Array Detector. *Microchem. J.* **2019**, *146*, 722–728. [[CrossRef](#)]
12. Bogireddy, N.K.R.; Cruz Silva, R.; Valenzuela, M.A.; Agarwal, V. 4-Nitrophenol Optical Sensing with N Doped Oxidized Carbon Dots. *J. Hazard. Mater.* **2020**, *386*, 121643. [[CrossRef](#)] [[PubMed](#)]
13. Konstantinou, G.N. Enzyme-Linked Immunosorbent Assay (ELISA). In *Food Allergens: Methods and Protocols*; Lin, J., Alcocer, M., Eds.; Methods in Molecular Biology; Springer: New York, NY, USA, 2017; pp. 79–94, ISBN 978-1-4939-6925-8.
14. Chu, Y.Y.; Qian, Y.; Wang, W.J.; Deng, X.L. A Dual-Cathode Electro-Fenton Oxidation Coupled with Anodic Oxidation System Used for 4-Nitrophenol Degradation. *J. Hazard. Mater.* **2012**, *199–200*, 179–185. [[CrossRef](#)] [[PubMed](#)]
15. Zhang, H.; Zhang, W.; Zhang, Z.; Shi, Z.; Liu, W. Green analytical method for the sensitive determination of mononitrophenol isomers by dynamic pH junction capillary electrophoresis. *J. Liq. Chromatogr. Relat.* **2014**, *37*, 1145–1162. [[CrossRef](#)]
16. Hao, T.; Wei, X.; Nie, Y.; Xu, Y.; Yan, Y.; Zhou, Z. An Eco-Friendly Molecularly Imprinted Fluorescence Composite Material Based on Carbon Dots for Fluorescent Detection of 4-Nitrophenol. *Microchim. Acta* **2016**, *183*, 2197–2203. [[CrossRef](#)]
17. Neng, N.R.; Nogueira, J.M.F. Determination of Phenol Compounds In Surface Water Matrices by Bar Adsorptive Microextraction-High Performance Liquid Chromatography-Diode Array Detection. *Molecules* **2014**, *19*, 9369–9379. [[CrossRef](#)] [[PubMed](#)]
18. Jiang, Y.; Zhao, H.; Liang, J.; Yue, L.; Li, T.; Luo, Y.; Liu, Q.; Lu, S.; Asiri, A.M.; Gong, Z.; et al. Anodic Oxidation for the Degradation of Organic Pollutants: Anode Materials, Operating Conditions and Mechanisms. A Mini Review. *Electrochem. Commun.* **2021**, *123*, 106912. [[CrossRef](#)]
19. Chang, G.; Luo, Y.; Lu, W.; Qin, X.; Asiri, A.M.; Al-Youbi, A.O.; Sun, X. Ag Nanoparticles Decorated Polyaniline Nanofibers: Synthesis, Characterization, and Applications toward Catalytic Reduction of 4-Nitrophenol and Electrochemical Detection of H<sub>2</sub>O<sub>2</sub> and Glucose. *Catal. Sci. Technol.* **2012**, *2*, 800–806. [[CrossRef](#)]
20. Manjula, N.; Chen, S.-M. Electrochemical Sensors for  $\beta$ -Adrenoceptor Agonist Isoprenaline Analysis in Human Urine and Serum Samples Using Manganese Cobalt Oxide-Modified Glassy Carbon Electrode. *New J. Chem.* **2021**, *45*, 9084–9095. [[CrossRef](#)]
21. Karimi-Maleh, H.; Karimi, F.; Fu, L.; Sanati, A.L.; Alizadeh, M.; Karaman, C.; Orooji, Y. Cyanazine Herbicide Monitoring as a Hazardous Substance by a DNA Nanostructure Biosensor. *J. Hazard. Mater.* **2022**, *423*, 127058. [[CrossRef](#)]
22. Karimi-Maleh, H.; Khataee, A.; Karimi, F.; Baghayeri, M.; Fu, L.; Rouhi, J.; Karaman, C.; Karaman, O.; Boukherroub, R. A Green and Sensitive Guanine-Based DNA Biosensor for Idarubicin Anticancer Monitoring in Biological Samples: A Simple and Fast Strategy for Control of Health Quality in Chemotherapy Procedure Confirmed by Docking Investigation. *Chemosphere* **2022**, *291*, 132928. [[CrossRef](#)] [[PubMed](#)]
23. Karimi-Maleh, H.; Orooji, Y.; Karimi, F.; Alizadeh, M.; Baghayeri, M.; Rouhi, J.; Tajik, S.; Beitollahi, H.; Agarwal, S.; Gupta, V.K.; et al. A Critical Review on the Use of Potentiometric Based Biosensors for Biomarkers Detection. *Biosens. Bioelectron.* **2021**, *184*, 113252. [[CrossRef](#)] [[PubMed](#)]
24. Ahmad, K.; Shinde, M.A.; Kim, H. Molybdenum Disulfide/Reduced Graphene Oxide: Progress in Synthesis and Electro-Catalytic Properties for Electrochemical Sensing and Dye Sensitized Solar Cells. *Microchem. J.* **2021**, *169*, 106583. [[CrossRef](#)]
25. Ahmad, K.; Kim, H. Fabrication of Nitrogen-Doped Reduced Graphene Oxide Modified Screen Printed Carbon Electrode (N-RGO/SPCE) as Hydrogen Peroxide Sensor. *Nanomaterials* **2022**, *12*, 2443. [[CrossRef](#)] [[PubMed](#)]
26. Ahmad, K.; Kumar, P.; Mobin. Hydrothermally grown novel pyramids of the CaTiO<sub>3</sub> perovskite as an efficient electrode modifier for sensing applications. *Mater. Adv.* **2020**, *1*, 2003–2009. [[CrossRef](#)]
27. Mohammad, A.; Ahmad, K.; Rajak, R.; Mobin, S.M. Binder Free Modification of Glassy Carbon Electrode by Employing Reduced Graphene Oxide/ZnO Composite for Voltammetric Determination of Certain Nitroaromatics. *Electroanalysis* **2018**, *30*, 274–282. [[CrossRef](#)]
28. Khan, M.Q.; Ahmad, K.; Alsalme, A.; Kim, H. Hydrothermal Synthesis of Nanostructured NiO for Hydrazine Sensing Application. *Mater. Chem. Phys.* **2022**, *289*, 126463. [[CrossRef](#)]
29. Abaker, M.; Dar, G.N.; Umar, A.; Zaidi, S.A.; Ibrahim, A.A.; Baskoutas, S.; Al-Hajry, A. CuO Nanocubes Based Highly-Sensitive 4-Nitrophenol Chemical Sensor. *Sci. Adv. Mater.* **2012**, *4*, 893–900. [[CrossRef](#)]
30. Ahmad, K.; Mobin, S.M. Shape Controlled Synthesis of High Surface Area MgO Microstructures for Highly Efficient Congo Red Dye Removal and Peroxide Sensor. *J. Environ. Chem. Eng.* **2019**, *7*, 103347. [[CrossRef](#)]
31. Ahmad, K.; Mohammad, A.; Mathur, P.; Mobin, S.M. Preparation of SrTiO<sub>3</sub> Perovskite Decorated RGO and Electrochemical Detection of Nitroaromatics. *Electrochim. Acta* **2016**, *215*, 435–446. [[CrossRef](#)]
32. Ahmad, K.; Mohammad, A.; Mobin, S.M. Hydrothermally Grown  $\alpha$ -MnO<sub>2</sub> Nanorods as Highly Efficient Low Cost Counter-Electrode Material for Dye-Sensitized Solar Cells and Electrochemical Sensing Applications. *Electrochim. Acta* **2017**, *252*, 549–557. [[CrossRef](#)]
33. Zhang, Y.; Huang, B.; Shao, Q.; Feng, Y.; Xiong, L.; Peng, Y.; Huang, X. Defect Engineering of Palladium–Tin Nanowires Enables Efficient Electrocatalysts for Fuel Cell Reactions. *Nano Lett.* **2019**, *19*, 6894–6903. [[CrossRef](#)] [[PubMed](#)]

34. Cheemalapati, S.; Palanisamy, S.; Mani, V.; Chen, S.-M. Simultaneous Electrochemical Determination of Dopamine and Paracetamol on Multiwalled Carbon Nanotubes/Graphene Oxide Nanocomposite-Modified Glassy Carbon Electrode. *Talanta* **2013**, *117*, 297–304. [[CrossRef](#)] [[PubMed](#)]
35. Jaiswal, N.; Tiwari, I.; Foster, C.W.; Banks, C.E. Highly Sensitive Amperometric Sensing of Nitrite Utilizing Bulk-Modified MnO<sub>2</sub> Decorated Graphene Oxide Nanocomposite Screen-Printed Electrodes. *Electrochim. Acta* **2017**, *227*, 255–266. [[CrossRef](#)]
36. Ahmad, K.; Mobin, S.M. Construction of polyaniline/ITO electrode for electrochemical sensor applications. *Mater. Res. Express* **2019**, *6*, 085508. [[CrossRef](#)]
37. Ahmad, K.; Mohammad, A.; Ansari, S.N.; Mobin, S.M. Construction of graphene oxide sheets based modified glassy carbon electrode (GO/GCE) for the highly sensitive detection of nitrobenzene. *Mater. Res. Express* **2018**, *5*, 075601. [[CrossRef](#)]
38. Ahmad, K.; Kumar, P.; Mobin, S.M. A Highly Sensitive and Selective Hydroquinone Sensor Based on a Newly Designed N-RGO/SrZrO<sub>3</sub> Composite. *Nanoscale Adv.* **2020**, *2*, 502–511. [[CrossRef](#)] [[PubMed](#)]
39. Wu, J.; Wang, Q.; Umar, A.; Sun, S.; Huang, L.; Wang, J.; Gao, Y. Highly Sensitive p -Nitrophenol Chemical Sensor Based on Crystalline  $\alpha$ -MnO<sub>2</sub> Nanotubes. *New J. Chem.* **2014**, *38*, 4420–4426. [[CrossRef](#)]
40. Xu, Y.; Wang, Y.; Ding, Y.; Luo, L.; Liu, X.; Zhang, Y. Determination of P-Nitrophenol on Carbon Paste Electrode Modified with a Nanoscaled Compound Oxide Mg(Ni)FeO. *J. Appl. Electrochem.* **2013**, *43*, 679–687. [[CrossRef](#)]
41. Sinhamahapatra, A.; Bhattacharjya, D.; Yu, J.-S. Green Fabrication of 3-Dimensional Flower-Shaped Zinc Glycerolate and ZnO Microstructures for p -Nitrophenol Sensing. *RSC Adv.* **2015**, *5*, 37721–37728. [[CrossRef](#)]
42. Chu, L.; Han, L.; Zhang, X. Electrochemical Simultaneous Determination of Nitrophenol Isomers at Nano-Gold Modified Glassy Carbon Electrode. *J. Appl. Electrochem.* **2011**, *41*, 687–694. [[CrossRef](#)]
43. Yang, C. Electrochemical Determination of 4-Nitrophenol Using a Single-Wall Carbon Nanotube Film-Coated Glassy Carbon Electrode. *Microchim. Acta* **2004**, *148*, 87–92. [[CrossRef](#)]
44. Casella, I.G.; Contursi, M. The Electrochemical Reduction of Nitrophenols on Silver Globular Particles Electrodeposited under Pulsed Potential Conditions. *J. Electrochem. Soc.* **2007**, *154*, D697. [[CrossRef](#)]
45. Dan, X.; Ruiyi, L.; Qinsheng, W.; Yongqiang, T.; Guangli, W.; Zaijun, L. Thermal-switchable sensor based on palladium-graphene composite and poly(N-isopropylacrylamide) for electrochemical detection of 4-nitrophenol. *Microchem. J* **2022**, *172*, 106970. [[CrossRef](#)]
46. Mohanta, D.; Mahanta, A.; Mishra, S.R.; Jasimuddin, S.; Ahmaruzzaman, M. Novel SnO<sub>2</sub>@ZIF-8/gC<sub>3</sub>N<sub>4</sub> nanohybrids for excellent electrochemical performance towards sensing of p-nitrophenol. *Environ. Res.* **2021**, *197*, 111077. [[CrossRef](#)]
47. Anbumannan, V.; Dinesh, M.; Kumar, R.T.R.; Suresh, K. Hierarchical  $\alpha$ -MnO<sub>2</sub> wrapped MWCNTs sensor for low level detection of p-nitrophenol in water. *Ceram. Int.* **2019**, *45*, 23097–23103. [[CrossRef](#)]
48. Wang, X.; Li, M.; Yang, S.; Bai, X.; Shan, J. Self-assembled Ti<sub>3</sub>C<sub>2</sub>T<sub>x</sub> MXene/graphene composite for the electrochemical reduction and detection of p-nitrophenol. *Microchem. J.* **2022**, *179*, 107473. [[CrossRef](#)]
49. Ren, D.; Wang, X.; Leng, C.; Meng, W.; Zhang, J.; Han, C. A Highly Sensitive Electrochemical Sensing Platform Based on P-doped Fe/Fe<sub>3</sub>O<sub>4</sub>@C for the Detection of 4-Nitrophenol. *J. Electrochem. Soc.* **2022**, *169*, 097501. [[CrossRef](#)]
50. Lei, L.; Li, C.; Huang, W.; Wu, K. Simultaneous detection of 4-chlorophenol and 4-nitrophenol using a Ti<sub>3</sub>C<sub>2</sub>T<sub>x</sub> MXene based electrochemical sensor. *Analyst* **2021**, *146*, 7593–7600. [[CrossRef](#)]
51. Dighole, R.P.; Munde, A.V.; Mulik, B.B.; Sathe, B.R. Bi<sub>2</sub>O<sub>3</sub> Nanoparticles Decorated Carbon Nanotube: An Effective Nanoelectrode for Enhanced Electrocatalytic 4-Nitrophenol Reduction. *Front. Chem.* **2020**, *8*, 325. [[CrossRef](#)]